Mineralogical Magazine, December 2016, Vol. 80(7), pp. 1205–1217

Dehydration phase transitions in new aluminium arsenate minerals from the Penberthy Croft mine, Cornwall, UK

Ian E. Grey[1,*], Helen E. A. Brand[2] and John Betterton[3]

[1] CSIRO Mineral Resources, Private bag 10, Clayton South, Victoria 3169, Australia
[2] Australian Synchrotron, 800 Blackburn Rd, Clayton, VIC 3168, Australia
[3] Haslemere Educational Museum, 78 High Street, Haslemere, Surrey GU27 2LA, UK

[*Received 2 March 2016; Accepted 25 May 2016; Associate Editor: Stuart Mills*]

ABSTRACT

Bettertonite, $[Al_6(AsO_4)_3(OH)_9(H_2O)_5]\cdot 11H_2O$ and penberthycroftite, $[Al_6(AsO_4)_3(OH)_9(H_2O)_5]\cdot 8H_2O$, two new minerals from the Penberthy Croft mine, Cornwall, have flexible layer structures based on corner-connected heteropolyhedral columns. Their response to dehydration on heating was studied using *in situ* synchrotron powder X-ray diffraction at temperatures in the range –53 to 157°C. The bettertonite sample transforms to penberthycroftite in a narrow temperature range of 67 to 97°C with a large (8%) contraction of the layer separation and a 6 Å sliding of adjacent layers relative to each other. Above 100°C a second phase transition occurs to a DL (displaced layer) phase, involving another 8% inter-layer contraction combined with a rotation of the columns. On heating the penberthycroftite sample the phase transition to the DL phase occurs at a lower temperature of ~80°C. The DL phase is stable to a temperature of ~120°C. At higher temperatures, increased rotation of the columns is accompanied by a progressive amorphization of the sample. Bettertonite, penberthycroftite and the DL phase exhibit negative thermal expansion (NTE) along all three axes with large NTE coefficients, of the order of -100×10^{-6} °C^{-1}.

Keywords: penberthycroftite, bettertonite, hydrated aluminium arsenates, dehydration phase transitions, *in situ* synchrotron powder diffraction.

Introduction

Two new secondary hydrated aluminium arsenate minerals have been described recently from the Penberthy Croft mine, located in the parish of St. Hilary, Cornwall, UK. They are bettertonite, $[Al_6(AsO_4)_3(OH)_9(H_2O)_5]\cdot 11H_2O$ (Grey *et al.*, 2015*a*) and penberthycroftite, $[Al_6(AsO_4)_3(OH)_9(H_2O)_5]\cdot 8H_2O$ (Grey *et al.*, 2016). The two minerals have related heteropolyhedral layer structures with similar monoclinic unit-cell parameters in the plane of the layers, $a \approx 7.8$ Å, $c \approx 15.8$ Å, but different interlayer spacings = $0.5b$ of 13.5 Å and 12.4 Å, respectively. The large decrease in the interlayer spacing is associated with a decrease in the interlayer water content, from $11H_2O$ to $8H_2O$ per formula unit. Projections along [100] of the two structures are compared in Fig. 1. The basic building block in the layers is a hexagonal ring of edge-shared octahedra with an AsO_4 tetrahedron attached to one side of the ring by sharing three basal corners as shown in Fig. 2(*a*). These polyoxometalate clusters, of composition $[AsAl_6O_{11}(OH)_9(H_2O)_5]^{8-}$, are interconnected along [100] and [001] by corner-sharing with other AsO_4 tetrahedra.

At the Penberthy Croft mine, bettertonite is found in close association with liskeardite, another secondary aluminium arsenate with a related composition, $[Al_{32}(AsO_4)_{18}(OH)_{42}(H_2O)_{22}]\cdot 52H_2O$ (Grey *et al.*, 2013). There is a close structural relationship between the [100] columns of hexagonal rings in bettertonite and penberthycroftite, and spiral columns in liskeardite, shown in Fig. 2*b*. Both columns have a 7.8 Å repeat distance and can be interconverted by the relocation of just one Al atom

*E-mail: ian.grey@csiro.au
DOI: 10.1180/minmag.2016.080.126

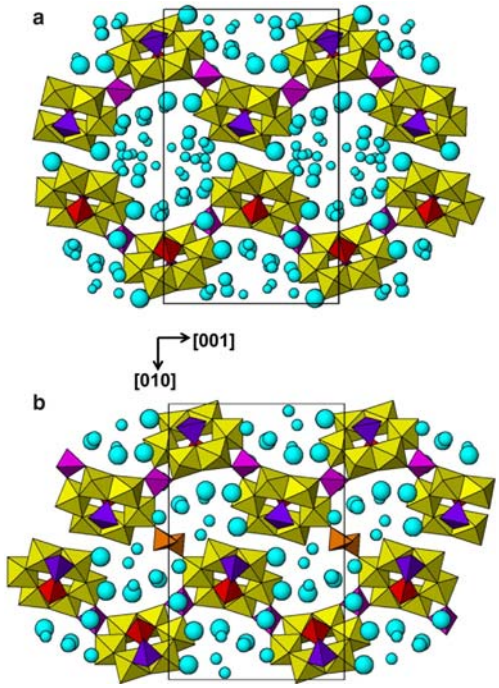

FIG. 1. Projections along [100] of the structures of (*a*) bettertonite and (*b*) penberthycroftite. The blue spheres are water molecules, with sizes proportional to the site occupancies. In (*b*) sulfate tetrahedra are brown. Axial directions shown are common to both structures.

per cluster as shown by the arrow in Fig. 2*b*. In liskeardite the spiral columns alternate with columns of pharmacoalumite structure to form orthogonally intersecting layers, giving an open framework structure, whereas in bettertonite and penberthycroftite only one orientation of layers is present

The heteropolyhedral layers are topologically identical in bettertonite and penberthycroftite, but they are displaced relative to one another by 6 Å along [001] in going from bettertonite to penberthycroftite. Because of the strongly undulating, crankshaft-like shape of the layers, the large layer offset along [001] results in a marked change in the interlayer volume available for water molecules. As shown in Fig. 1, bettertonite has large elliptical channels measuring ~8 Å × 13 Å centred at $y = 0$, $z = ½$ and $y = ½$, $z = 0$, whereas penberthycroftite has much smaller channels, ~6 Å × 7 Å, located on either side of the above positions, containing a correspondingly lower water content in the channels.

The two minerals have similar forms, occurring as ultrathin (sub micrometre) rectangular laths that are flattened on {010} and elongated on [100], and they occur in close proximity to one another in hand specimens. This raises the question: did one mineral form from the other by hydration/dehydration or did they individually form under locally different conditions? Also, given that bettertonite and penberthycroftite are related by a relative sliding of adjacent layers, are there other potential minerals that can form on hydration/dehydration that involve different relative locations of the layers? To address these questions we have conducted *in situ* synchrotron powder X-ray diffraction (XRD) experiments on the dehydration reactions of both minerals. We have recently reported the results of a similar study on liskeardite that showed that the mineral undergoes a dramatic (volume decrease of 30%) 2D contraction of the framework when dehydrated by heating to 100°C, and above 100°C the transformed liskeardite shows unprecedented negative thermal expansion (NTE) of the axes defining the framework, of the order of -900×10^{-6} °C^{-1} (Grey *et al.*, 2015*b*). The observed NTE is due to cooperative rotation of the heteropolyhedral columns in liskeardite via the octahedral-tetrahedral corner-linkages, and as bettertonite and penberthycroftite have similar inter-column linkages it was anticipated that they may show similar NTE behaviour.

Experimental

Samples

Hand specimens containing the bettertonite and penberthycroftite used in this study were collected by one of us (JB) during the early 2000s on the mine dumps associated with the Penberthy Croft mine. The specimens are distributed very sparsely in cavities on massive quartz and are associated intimately with very thin quartz and chamosite in the case of penberthycroftite, and with fine-grained pharmacosiderite in the case of bettertonite. After removal of the visible associated minerals under a binocular microscope, quantities of very fine fragments of the impurities remained and were taken into account in Rietveld fitting of the diffraction patterns for heated bettertonite and penberthycroftite. Chemical analyses of both minerals are reported by Grey *et al.* (2015*a*, 2016). In addition to the main elements, small amounts of Fe and S (~1 wt.% S) were analysed in both minerals. The S was located structurally as $(SO_4)^{2-}$ anions coordinated to Al in

https://doi.org/10.1180/minmag.2016.080.126 Published online by Cambridge University Press

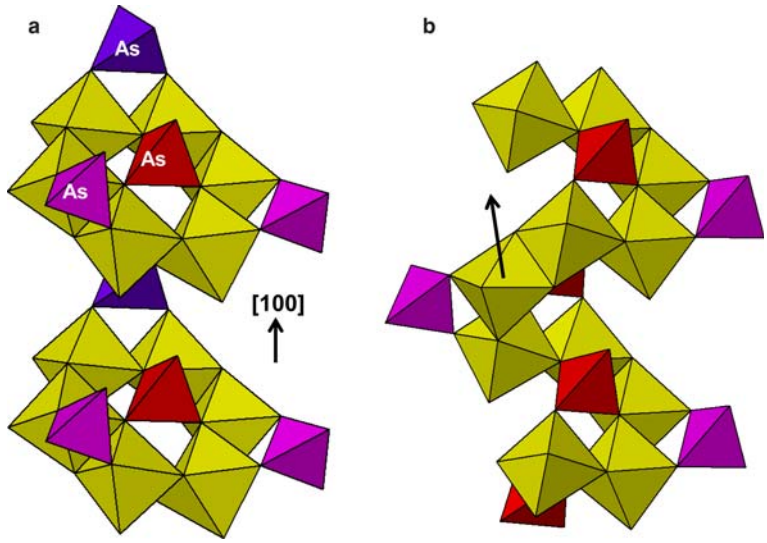

FIG. 2. A comparison of the layer-building [100] heteropolyhedral columns in (*a*) bettertonite and penberthycroftite and (*b*) liskeardite. The arrow in (*b*) shows the movement of an Al-centred octahedron required to transform the column in liskeardite to that in bettertonite.

penberthycroftite (Grey *et al.*, 2016), but not in bettertonite, where its location must be disordered.

Thermal analyses

A thermogravimetric (TG) analysis of penberthycroftite was conducted using a Netzsch STA 449 F1 Jupiter Simultaneous TGA/DSC Thermal Analyser, in conjunction with a Thermostar Pfeiffer mass spectrometer (MS) to analyse the gases evolved. The sample was contained in an alumina crucible and heated from ambient to 600°C in flowing air, at a heating rate of 10°C min^{-1}. Because of the sparse occurrences of the mineral, the sample weight was restricted to <2 mg and the TG results were compromised by buoyancy errors. Satisfactory DSC and MS results were obtained however.

Synchrotron powder XRD

Lightly ground samples were packed in 0.3 mm diameter quartz glass capillaries for powder XRD data collections, which were conducted on the powder diffraction beamline at the Australian Synchrotron (Wallwork *et al.*, 2007). High energy 18 keV X-rays were used to reduce fluorescence due to As. The wavelength was 0.68824(1) Å, calibrated to NIST standard LaB_6 660b. The capillary was positioned in the diffractometer rotation centre and spun at ~1 Hz. The X-ray beam was aligned to coincide with the diffractometer centre. The data were collected using a Mythen position sensitive detector (Schmitt *et al.*, 2003) covering 80° in 2θ with a resolution of 0.004° in 2θ. Heating and cooling was supplied by an Oxford Cryostream system. The first data collection was at ambient. The temperature was then lowered to –53° C (220 K) and patterns were collected at 30°C intervals on heating to 67°C, followed by 10° intervals to 157°C, at which temperature the dehydration product had become largely amorphous. At each temperature pairs of data sets were collected at two detector positions 0.5° apart in order to cover the gaps between the detector modules. Acquisition time at each position was 300 s. The data pairs were merged into single files using in-house data processing software, *PDViPcR*, available at the beamline.

Ex situ laboratory powder XRD

A few experiments were conducted in an open environment to check on reversal of the dehydration. Ground samples were spread on a silicon disk and heated in an oven at different temperatures up to 125°C. The heated samples were cooled in a dessicator and then diffraction patterns were recorded using a Philips diffractometer with

https://doi.org/10.1180/minmag.2016.080.126 Published online by Cambridge University Press

graphite-monochromated Co$K\alpha$ radiation. The patterns were then repeated after exposure to air at ambient conditions.

Rietveld refinements

Rietveld refinements were conducted using *FULLPROF* (Rodriguez-Carvajal, 1990). Undulations in the background due to capillary contributions were modelled by interpolation between 38 measured and refinable background points. Although diffraction data were collected to 80° in 2θ, the peak intensities for both minerals dropped markedly beyond 2θ = 17° (d = 2.3 Å) and could not be distinguished above background beyond 2θ = 33° (d = 1.2 Å), so the data used in the refinements was restricted to $2\theta_{max} = 33°$.

Structural parameters in the space group $P2_1/c$ for both minerals were taken from the single crystal refinements (Grey *et al.*, 2015*a*, 2016). Due to the low data resolution and the very large, low-symmetry structures of both bettertonite and penberthycroftite (59 and 49 independent non-hydrogen atoms, respectively) the structural parameters were fixed at the single-crystal values for refinement of the heated samples. The most important information to be gained from such heating studies is the precise determination of unit-cell parameter variations. Refinement variables were restricted to the unit-cell parameters and profile parameters. The latter included a pseudo-Voigt shape function, the scale factor, two half-width parameters, and a zero-shift parameter. Quartz was included as a second phase in the refinements of penberthycroftite, while quartz and pharmacosiderite were both included in the refinements of bettertonite.

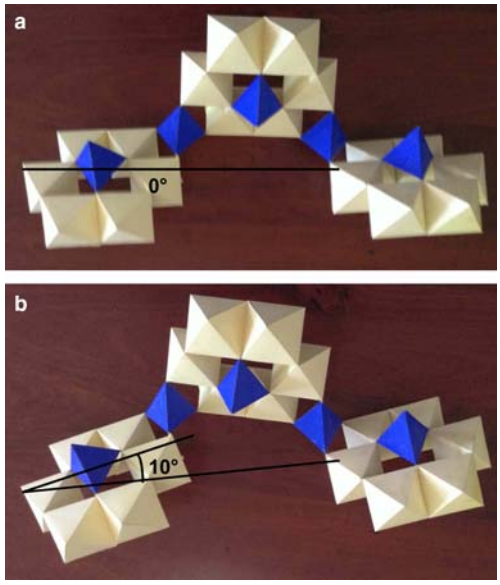

FIG. 3. Demonstration of rotation of [100] heteropolyhedral columns about As–O–Al corner linkages using cardboard models. (*a*) Zero rotation, (*b*) columns rotated by 10°, as in bettertonite and penberthycroftite.

Structural model for heated penberthycroftite

Heating penberthycroftite above 80°C brought about a sudden step-change in XRD peak positions that could be indexed with a similar monoclinic cell to that for penberthycroftite, but with large decreases in the b (7.6%) and c (3.0%) unit-cell parameters. The decrease in b is comparable to the decrease in b from bettertonite to penberthycroftite

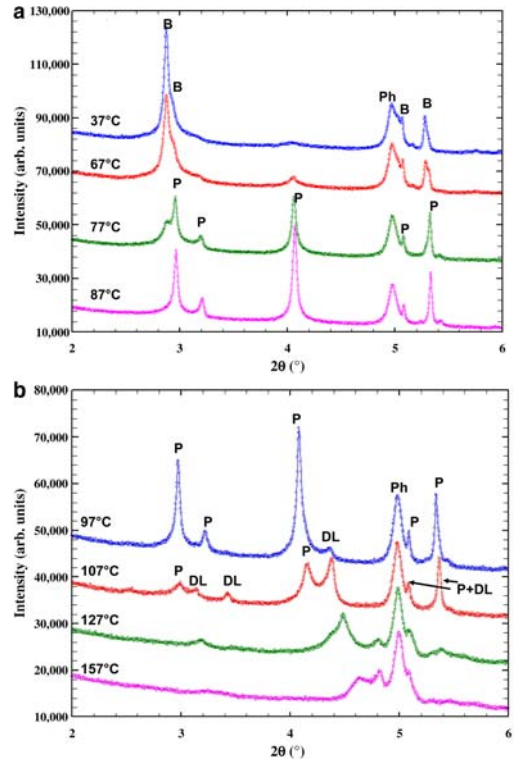

FIG. 4. Low-angle region of selected powder XRD patterns for heated bettertonite. (*a*) For temperatures of 37 to 87°C and (*b*) for temperatures of 97 to 157°C. Labels are B = bettertonite, P = penberthycroftite, Ph = pharmacosiderite and DL = displaced layer phase.

https://doi.org/10.1180/minmag.2016.080.126 Published online by Cambridge University Press

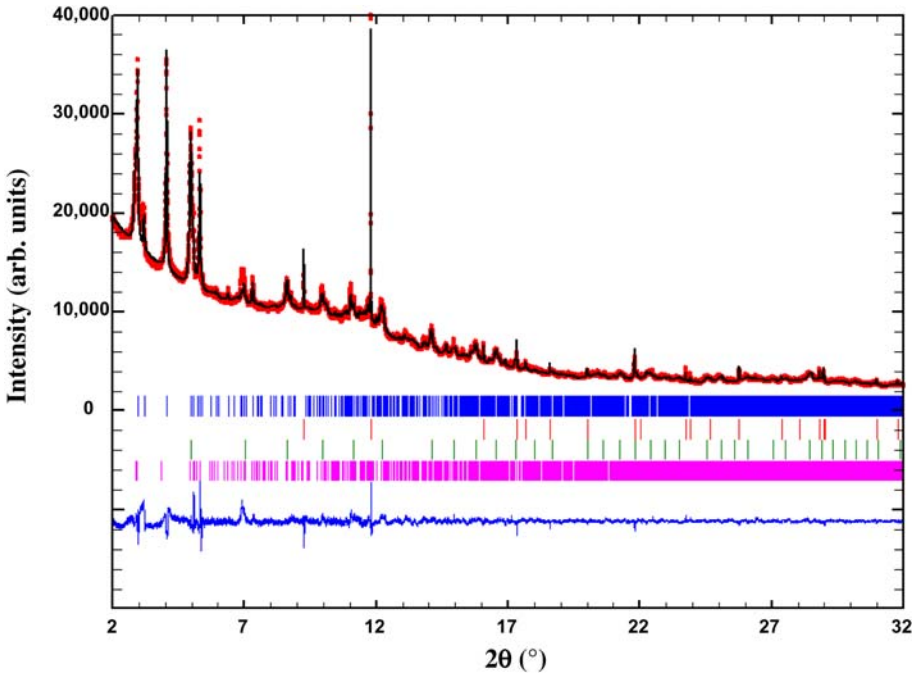

FIG. 5. Rietveld fit (black line) to powder XRD data (red dots) for bettertonite heated to 77°C. The tick marks refer to the peak positions for (in descending order) penberthycroftite, quartz, pharmacosiderite and bettertonite. A difference plot is shown below.

and can be understood in terms of a further sliding and contraction of the heteropolyhedral layers relative to one another. On this basis we refer to the high temperature phase as DL, for 'displaced layer' phase. The decrease in *c* in the transformation from penberthycroftite to DL is much larger than that between bettertonite and penberthycroftite. It can be explained by a rotation of the [100] columns shown in Fig. 2*a* about the corner-linkages with the bridging AsO_4 groups. This type of cooperative rotation of columns occurs when the related mineral liskeardite is heated (Grey *et al.*, 2015*b*). The rotational flexibility was confirmed by applying different rotations to cardboard models of the heteropolyhedral layers, illustrated in Fig. 3. This shows a layer in the fully extended state in Fig. 3*a*, and after rotation of individual columns by 10° about [100] in Fig. 3*b*. The latter corresponds to the column rotation in both bettertonite and penberthycroftite, Fig. 1. On the basis that the separation between the linking AsO_4 tetrahedra remains constant during rotation, the magnitude of rotation required to give the observed *c*-axis shrinkage on formation of the DL phase is readily calculated to be ~7° relative to that in penberthycroftite.

A starting structural model for the DL phase in space group $P2_1/c$ was then generated from the published structural coordinates for penberthycroftite by applying a 7° rotation about [100] to the heteropolyhedral column shown in Fig. 2*a*. The rotation calculation was made in Excel, and corrections were also applied to the coordinates to allow for the smaller unit-cell parameters in the DL phase. The program *ATOMS* was used to check that the Al and As atom coordinations remained unchanged by the rotation and cell-shrinkage operations. The sliding of the layers relative to one another was accomplished during a Rietveld refinement by treating the heteropolyhedral columns as rigid bodies and constraining the coordinate shifts along *x*, *y* and *z* to be the same for all atoms in the asymmetric unit. Interlayer water molecules were located during the Rietveld refinements from difference-Fourier maps and their positions were not refined. The restriction of the number of refinable parameters was very important because of the low resolution of the XRD data and the presence of platy quartz and chamosite with strong texture effects as impurity phases. In the Rietveld refinements the resolution was restricted to

https://doi.org/10.1180/minmag.2016.080.126 Published online by Cambridge University Press

TABLE 1. Refined unit-cell parameters and unit-cell volumes of phases during the heating of bettertonite.

t, °C	Phase(s)	a (Å)	b (Å)	c (Å)	β (°)	V(Å^3)
−53	B	7.789(1)	26.902(3)	15.958(1)	93.98(1)	3336(1)
	Ph	7.928(1)				498.3(2)
−23	B	7.793(1)	26.909(3)	15.971(1)	93.97(1)	3341(1)
	Ph	7.931(1)				498.9(2)
7	B	7.797(1)	26.921(3)	15.990(1)	93.96(1)	3348(1)
	Ph	7.934(1)				499.4(2)
37	B	7.797(1)	26.943(3)	15.997(1)	93.94(1)	3353(1)
	Ph	7.935(1)				499.6(2)
67	B*	7.786(1)	26.913(4)	15.987(2)	93.87(1)	3342(1)
	Ph	7.930(1)				498.7(2)
77	B (minor)	7.770(2)	26.90(2)	15.965(9)	94.01(5)	3328(6)
	P(major)	7.785(1)	24.599(2)	15.884(2)	93.49(1)	3036(1)
	Ph	7.927(1)				498.2(2)
87	P	7.774(1)	24.547(2)	15.866(1)	93.40(1)	3022(1)
	Ph	7.923(1)				497.4(2)
97	P	7.766(1)	24.453(2)	15.832(2)	93.35(1)	3001(1)
	Ph	7.919(1)				496.6(2)
107	P	7.759(2)	23.812(7)	15.757(6)	93.59(3)	2905(3)
	DL	7.799(1)	22.885(7)	14.863(7)	95.76(3)	2639(3)
	Ph	7.917(1)				496.2(2)
157	Ph	7.901(1)				493.2(2)

*minor P present.

2.3 Å (17° in 2θ) and the quartz and chamosite peaks were excluded from the refinement. Even at the low resolution, because of the large, low-symmetry cell, 215 peaks are present to be fitted for the DL phase.

Results

Heating of bettertonite

Selected diffraction patterns corresponding to heating of bettertonite at temperatures between 37 and 87°C are shown in Fig. 4*a*. At 67°C, sharp peaks due to penberthycroftite first appear. Penberthycroftite becomes the major phase at 77°C, and completely replaces bettertonite at 87°C. The temperature region 67 to 87°C thus corresponds to a 2-phase mixture of bettertonite and penberthycroftite, in which adjacent layers in bettertonite are displaced by 6 Å. Peaks corresponding to structures with intermediate relative displacements of the layers were not evident. The stability region for penberthycroftite is very narrow. At 97°C peaks due to a new phase appear and at 107°C, penberthycrofite becomes a minor phase, shown in Fig. 4*b*. The new phase, labelled 'DL', corresponds to a further displacement of the layers relative to one another along [001] and a contraction normal to (010). This phase is better defined in the heating experiments on penberthycroftite, and so discussion of it is given in a later section. By 127°C peaks due to penberthycroftite were completely gone and peaks due to the DL phase moved to higher angles and weakened. By 157°C, extensive amorphization had occurred, as evidenced by the pharmacosiderite peak at 2θ = 5° in Fig. 4*b* becoming the strongest peak in the pattern.

Rietveld refinements were conducted on the scans obtained by heating bettertonite at all temperatures between –53°C and 107°C. Despite restricting the refinement parameters to profile and unit-cell parameters only, good fits were obtained as illustrated for the case of heating at 77°C in Fig. 5. In this case the data were fitted with four phases: bettertonite, penberthycroftite, pharmacosiderite and quartz. The resulting fit parameters were $R_{wp} = 3.26$ and $\varphi^2 = 7.2$. Quantitative phase analysis using *FULLPROF* (Rodriguez-Carjaval,

https://doi.org/10.1180/minmag.2016.080.126 Published online by Cambridge University Press

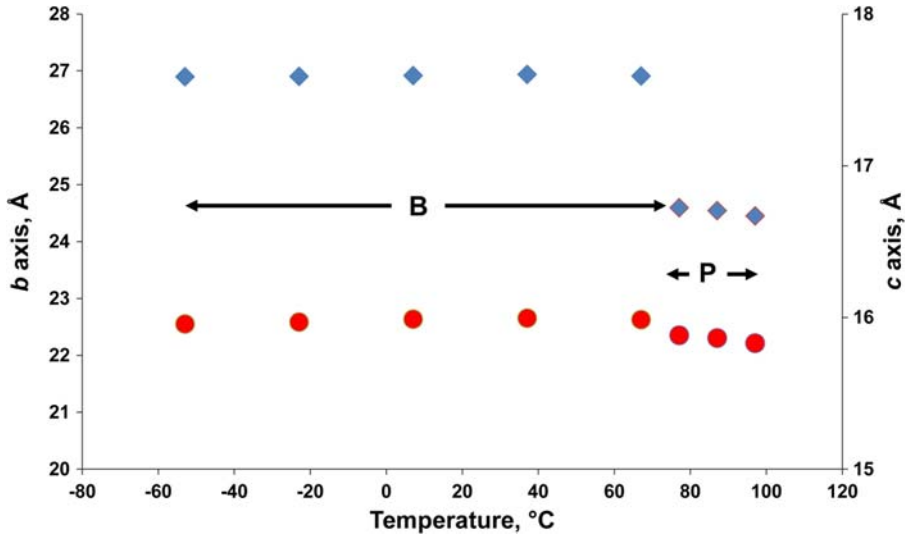

FIG. 6. Variation of *b* (diamonds) and *c* (circles) unit-cell parameters with temperature for bettertonite (B) and penberthycroftite (P), from Rietveld refinement of XRD scans obtained by heating bettertonite.

1990) gave 45% penberthycroftite, 22% bettertonite, 21% pharmacosiderite and 12% quartz.

Refined unit-cell parameters and unit-cell volumes are reported in Table 1. The *b* and *c* parameters are plotted in Fig. 6. As seen from Table 1, the changes in the *a* parameter with temperature are much smaller. Figure 6 illustrates the large step-decrease in *b* (by 8.6%) when bettertonite transforms to penberthycroftite. The *c* parameter also undergoes contraction across the transition but it is much smaller (0.6%). The volume decrease from bettertonite to penberthycroftite at 77°C is 8.8%. The unit-cell parameters for bettertonite expand linearly with increasing temperature from –53 to 37°. At temperatures above 37°C the thermal expansion of bettertonite is reversed and all three unit-cell parameters display NTE. The thermal expansion coefficients are reported in Table 2. These show large NTE values for penberthycroftite, with the contraction of the *b* axis being twice as large as the contractions of *a* and *c*.

The refined cubic unit-cell parameter for associated pharmacosiderite is also reported in Table 1. Similarly to bettertonite, the unit-cell parameter expands with temperature up to ambient and then undergoes NTE. Pharmacosiderite, $(K,H_3O)Fe_4(AsO_4)_3(OH)_4{\cdot}4H_2O$, has an open framework structure in which tetrameric clusters of edge-sharing octahedra are interconnected via corner sharing with AsO_4 tetrahedra (Buerger *et al.*, 1967). The NTE behaviour is most likely due to flexing (rotation) about these corner-linkages, analogous to that reported for liskeardite (Grey *et al.*, 2015*b*). The pharmacosiderite phase was stable up to the highest temperature used in this study of 157°C. The NTE coefficient is linear over the temperature range of 67 to 157°C, with $\alpha = -40 \times 10^{-6}\ °C^{-1}$. It is larger by a factor of 4 compared to the classic cubic NTE material ZrW_2O_6 (Evans, 1999) and is also considerably higher than reported NTE coefficients for a range of zeolites (Lightfoot *et al.*, 2001).

Heating of penberthycroftite

Selected diffraction patterns showing the main phase changes during the heating of penberthycroftite are shown in Fig. 7. Penberthycroftite remains stable with heating up to 77°C, at which temperature there is the first appearance of peaks that correspond to a new phase. This phase is labelled 'DL' in Fig. 7. The phase transition is rapid, and only a trace of penberthycroftite remains after heating to 87°C. The DL phase is stable up to 117°C. At 127°C the DL peaks diminish by about one third and peaks due to another new phase appear. These are labelled 'Rot' in Fig. 7, corresponding to a phase with increased rotation of the [100] heteropolyhedral columns that form the layers. At higher temperatures the peaks become very weak and broad, corresponding to progressive amorphization of the sample, shown for the scan at 147°C in Fig. 7. On return of

https://doi.org/10.1180/minmag.2016.080.126 Published online by Cambridge University Press

TABLE 2 Linear thermal expansion coefficients ($\times 10^6$ $°C^{-1}$).

Phase	Temp. range, °C	*a*	*b*	*c*
Heating of bettertonite				
B	−53 to 37	+10	+15	+30
B	37 to 77	−70	−40	−40
P	77 to 97	−130	−300	−160
Ph	−53 to 37	+10		
Ph	37 to 147	−45		
Heating of penberthycroftite				
P	−53 to 37	+15	+20	+15
P	37 to 77	−40	−90	−20
DL	87 to 137	−90	−220	−185

the temperature of the sample to ambient, the pattern remained unchanged.

Based on the movement of peaks during the phase transition from penberthycroftite to DL, the DL phase patterns were readily indexed using a monoclinic cell related to that of penberthycroftite, but with a large (7.6%) decrease in *b* and a smaller (3%) decrease in *c*. A structural model for the DL phase was developed as described above, and used in Rietveld refinements of the scans in which the DL phase was present. An example of the Rietveld fit to the synchrotron XRD data for the DL phase formed at 97°C is shown in Fig. 8. Given that individual atom positions were not refined, but only group *x*, *y* and *z* coordinates for the rotated [100] columns as rigid bodies, the fit is reasonable with $R_{wp} = 2.54$ and $\varphi^2 = 6.7$. The structural coordinates for the DL phase obtained by the combination of column rotations and Rietveld refinement of column translations are given in Table 3. A [100] projection of the structure of the DL phase is shown in Fig. 9. A comparison with the structures of penberthycroftite and bettertonite in Fig. 1 shows the effect of the increased column rotation on the layer packing and inter-layer space.

At a temperature of 127°C the XRD pattern showed diminished peaks due to the DL phase and the appearance of new peaks that could be indexed with a monoclinic cell having similar *a* and *b* parameters to the associated DL phase, but with a significant reduction (>3%) in the *c* parameter. We interpreted the structure of this phase, labelled 'Rot' in Fig. 7, as being related to the DL phase in having

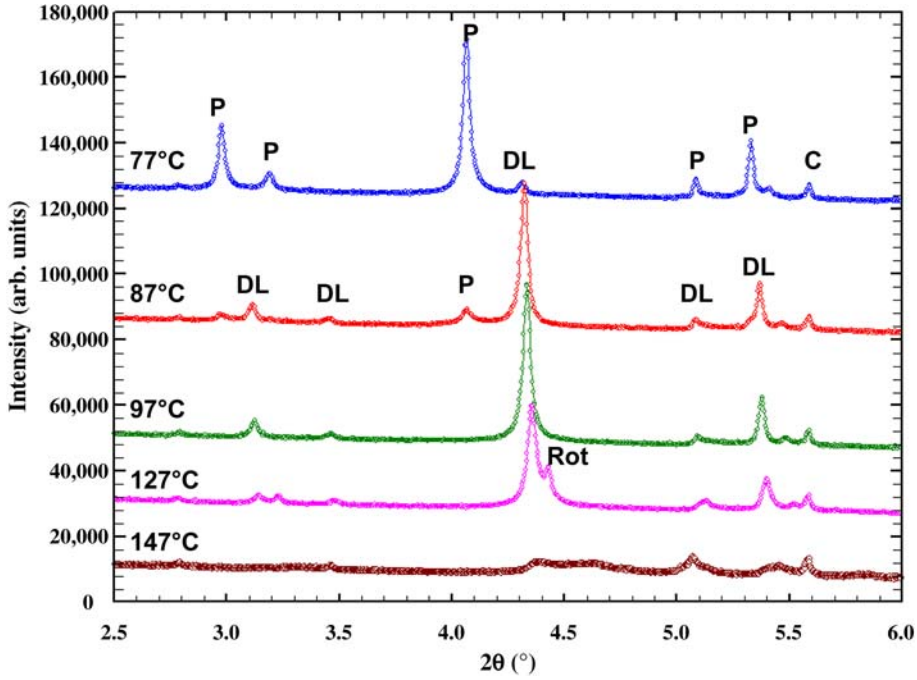

FIG. 7. Low-angle region of selected powder XRD patterns for heated penberthycroftite. Labels as in Fig. 4. C = chamosite, Rot = phase with increased rotation of [100] columns relative to the DL phase.

https://doi.org/10.1180/minmag.2016.080.126 Published online by Cambridge University Press

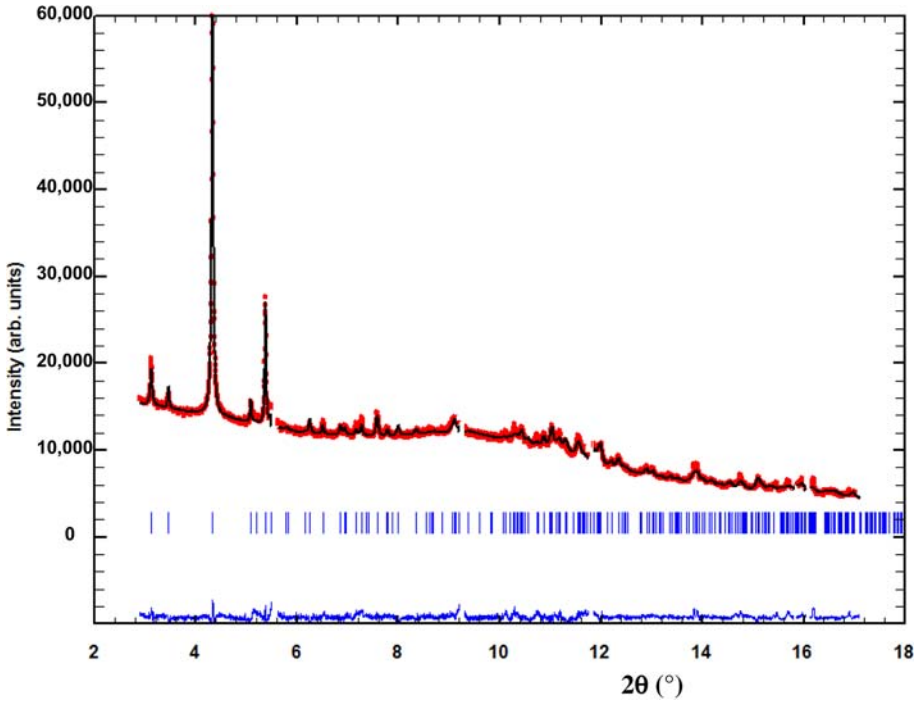

FIG. 8. Rietveld fit (black line) to powder XRD data (red dots) for the DL phase formed by heating penberthycroftite to 97°C. The tick marks refer to the peak positions for the DL phase. A difference plot is shown below. Gaps in the pattern are where peaks due to quartz and chamosite impurities have been excluded.

a similar layer spacing but having a larger rotation of the [100] columns. From the shrinkage of *c* the rotation angle was calculated to be 14.3° relative to penberthycroftite, or 7.3° relative to the DL phase. The scans obtained at 127 and 137°C were fitted using 2-phase mixtures of structural models for the DL and Rot phases. At higher temperatures the Rot-phase peaks became progressively broader and weaker and were not able to be fitted reliably. A marked deterioration of the Rietveld fit to the scan at 137°C, where the Rot phase is the major phase, suggested also that the monoclinic $P2_1/c$ symmetry may not be adequate to fit the structure at high rotation angles.

The unit-cell parameters and unit-cell volumes obtained from the Rietveld refinements of scans from –53 to 137°C are reported in Table 4 and the *b* and *c* parameters are plotted *vs*. temperature in Fig. 10. This Figure shows clearly the step-decreases in both *b* and *c* when penberthycroftite transforms to the DL phase, whereas the further rotations of the columns in the Rot phase result in a step-decrease in *c* but not in *b*. The results in Table 4 show that penberthycroftite undergoes normal thermal expansion from –53 to 37°C but exhibits NTE of all three axes at temperatures above 37°C. The DL phase also exhibits strong NTE along all three axes, with considerably higher NTE coefficients than for penberthycroftite, as reported in Table 2.

The structural changes to penberthycroftite on heating can be linked to dehydration via thermal analysis. The differential scanning calorimetry (DSC) curve in Fig. 11 shows a broad endotherm extending from 50 to 150°C, peaking at 95°C. The mass spectrum (MS) for evolved H_2O also peaks at 95°C, confirming that the endotherm is due to water loss. The temperature range of the endotherm corresponds to the observed range over which penberthycroftite transforms to the DL phase and then to the Rot phase. By ~150°C it can be inferred that the rotational flexing of the layers corresponds to the complete expulsion of interlayer water molecules. A second endotherm and corresponding MS H_2O peak occurs at 185°C. Almost the same thermal features were reported for the dehydration of liskeardite (Grey *et al.*, 2015*b*). For this mineral, larger quantities of pure material were available and

https://doi.org/10.1180/minmag.2016.080.126 Published online by Cambridge University Press

TABLE 3. Atomic coordinates for DL phase at 97°C*

Atom	*x*	*y*	*z*
AS1	0.4662(8)	0.6726(3)	0.2997(4)
AS2	0.9578(8)	0.5777(3)	0.3449(4)
AS3	0.2568(8)	0.6852(3)	0.0244(4)
AL1	0.0700(8)	0.6657(3)	0.1973(4)
AL2	0.6193(8)	0.5894(3)	0.4479(4)
AL3	0.5907(8)	0.5339(3)	0.2565(4)
AL4	0.3280(8)	0.5739(3)	0.1352(4)
AL5	0.3780(8)	0.6806(3)	0.5068(4)
AL6	0.0965(8)	0.7187(3)	0.3820(4)
S1	0.3514(8)	0.4522(3)	0.0067(4)
O1	0.3194(8)	0.6488(3)	0.2171(4)
O2	0.5680(8)	0.6131(3)	0.3277(4)
O3	0.3480(8)	0.6978(3)	0.3848(4)
O4	0.6000(8)	0.7213(3)	0.2722(4)
O5	0.8620(8)	0.5904(3)	0.4387(4)
O6	0.8290(8)	0.5402(3)	0.2640(4)
O7	0.0150(8)	0.6449(3)	0.3139(4)
O8	1.1290(8)	0.5379(3)	0.3624(4)
O9	0.3416(8)	0.6203(3)	0.0413(4)
O10	0.1523(8)	0.7958(3)	0.4305(4)
O11	0.4086(8)	0.7626(3)	0.5459(4)
O12	0.1065(8)	0.7057(3)	0.0975(4)
OH1	0.0873(8)	0.5873(3)	0.1430(4)
OH2	0.0902(8)	0.7384(3)	0.2684(4)
OH3	0.6160(8)	0.6689(3)	0.5051(4)
OH4	0.3886(8)	0.5978(3)	0.4731(4)
OH5	0.5814(8)	0.5151(3)	0.3787(4)
OH6	0.5674(8)	0.5658(3)	0.1530(4)
OH7	0.3460(8)	0.5287(3)	0.2314(4)
OH8	0.1400(8)	0.6848(3)	0.4868(4)
Ow1	−0.1630(8)	0.6706(3)	0.1678(4)
Ow2	0.6480(8)	0.5509(3)	0.5532(4)
Ow3	0.6150(8)	0.4530(3)	0.2044(4)
Ow4	0.2910(8)	0.5074(3)	0.0482(4)
Ow5	0.3580(8)	0.6612(3)	0.6207(4)
Ow6	−0.1410(8)	0.7340(3)	0.3963(4)
Os1	0.2290(8)	0.4295(3)	−0.0652(4)
Os2	0.3690(8)	0.4097(3)	0.0704(4)
Os3	0.4380(8)	−0.0064(3)	0.5492(4)
W1	0.720	0.823	0.512
W2	0.899	0.415	0.338
W3	0.452	0.687	0.770

*From Rietveld refinement, $R_{wp} = 2.54$, $\varphi^2 = 6.7$.
Space group $P2_1/c$, unit-cell parameters given in Table 4.
Ow = coordinated water, W = interlayer water, Os = SO_4 oxygen.

reliable mass-loss measurements were obtained which confirmed that the first DSC peak is due to loss of exra-framework water and the second peak is due to the loss of water coordinated to Al. The DSC curve for heated penberthycroftite also shows an exotherm at 515°C. The MS results confirmed that this coincided with loss of sulfur. No loss of As was recorded in the temperature range used.

Discussion

The *in situ* heating experiments on bettertonite confirm that it transforms on heating to penberthycroftite. The first indication of the formation of penberthycroftite occurred at a temperature of 67°C as shown in Fig. 4. The time to reach a temperature of 67° from ambient in the *in situ* heating experiments was only of the order of 30 min. Longer heating times, as occurs in the field, could result in the transformation occurring at a lower temperature. Temperatures close to 60°C have been measured in mine dumps containing pyritic material, due to local heating associated with the oxidation of the sulfide minerals (Harries and Ritchie, 1981). Pyrite and arsenopyrite are abundant at Penberthy Croft (Betterton, 2000) and the formation of a diverse suite of secondary arsenate minerals at the mine, including bettertonite and penberthycroftite, is attributed to oxidation and further reactions of the arsenopyrite. It is likely that local temperatures due to sulfide oxidation have been high enough for the bettertonite to transform to penberthycroftite.

The unit cell for penberthycroftite obtained by heating bettertonite differs significantly from that for as-received penberthycroftite, with the former having a *b* parameter 0.4% smaller and a *c* parameter 0.95% larger. This may be at least partly due to different levels of minor substitution of Fe for Al in the two minerals, with 2.5% Fe_2O_3 in bettertonite (Grey *et al.*, 2015*a*) and only 0.45% Fe_2O_3 in penberthycroftite (Grey *et al.*, 2016). Another factor may be the role of coordinated SO_4. The two minerals contain similar levels of S. It was found, however, to be ordered as SO_4 coordinated to one Al site in penberthycroftite but was not located in bettertonite, despite the quality of the single-crystal XRD data being similar for both minerals. It is likely that in bettertonite, with its expanded interlayer region, the SO_4 is disordered over multiple sites.

Natural penberthycroftite and penberthycroftite formed by heating bettertonite exhibit quite different structural responses on heating. Natural penberthycroftite starts transforming to the DL phase at 77°C and the DL phase remains as a single phase up to at least 120°C, whereas penberthycroftite formed from bettertonite does not start transforming to the DL phase until nearly 100°C.

https://doi.org/10.1180/minmag.2016.080.126 Published online by Cambridge University Press

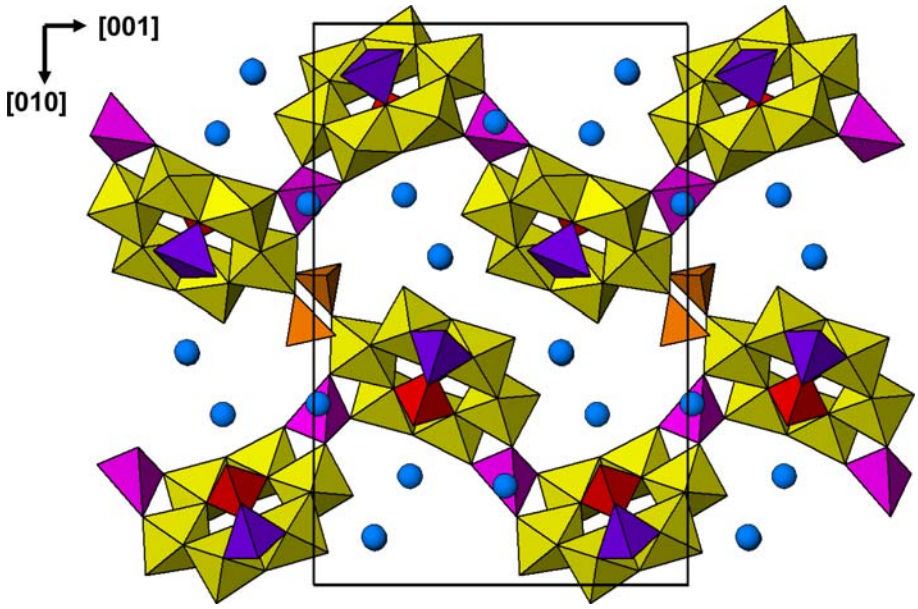

FIG. 9. Projection along [100] of the structure of the DL phase.

The DL phase was not present as a single phase at any stage in heated bettertonite. At 107 and 117°C the DL phase and penberthycroftite co-existed while at 127°C the DL phase had largely converted to the Rot phase. A further difference, evident from Table 2, is that the NTE coefficients for penberthycroftite formed by heating bettertonite are much larger, by almost an order of magnitude for *c*, than those for natural penberthycroftite. The different Fe levels and the different thermal response of the structure of natural penberthycroftite compared with the structure for penberthycroftite formed from bettertonite tend to support the premise that the penberthycroftite did not form by dehydration of bettertonite, but formed separately.

The transformation of penberthycroftite to the DL phase on dehydration raises the possibility that the DL phase could exist as a mineral. X-ray

TABLE 4. Refined unit-cell parameters and unit-cell volumes of phases during the heating of penberthycroftite.

T, °C	Phase(s)	*a* (Å)	*b* (Å)	*c* (Å)	β (°)	*V* (Å^3)
−53	P	7.783(1)	24.760(2)	15.725(1)	93.98(1)	3023(1)
−23	P	7.787(1)	24.766(2)	15.735(2)	93.94(1)	3027(1)
7	P	7.791(1)	24.791(3)	15.741(2)	93.91(1)	3033(1)
37	P	7.792(1)	24.798(3)	15.747(2)	93.89(1)	3036(1)
67	P	7.785(1)	24.742(3)	15.737(2)	93.90(1)	3024(1)
77	P	7.779(1)	24.704(3)	15.733(2)	93.87(1)	3017(1)
87	DL	7.787(1)	22.829(1)	15.257(1)	94.77(1)	2703(1)
97	DL	7.779(1)	22.773(1)	15.221(1)	95.03(1)	2686(1)
107	DL	7.773(1)	22.732(1)	15.207(1)	95.17(1)	2676(1)
117	DL	7.767(1)	22.688(1)	15.188(5)	95.40(1)	2665(1)
127	DL (major)	7.760(1)	22.667(2)	15.128(2)	95.65(1)	2648(1)
	Rot (minor)	7.730(1)	22.630(2)	14.620(2)	94.76(1)	2549(1)
137	DL (minor)	7.754(1)	22.547(8)	15.120(7)	96.26(1)	2628(2)
	Rot (major)	7.724(1)	22.510(6)	14.613(6)	94.71(4)	2532(2)

https://doi.org/10.1180/minmag.2016.080.126 Published online by Cambridge University Press

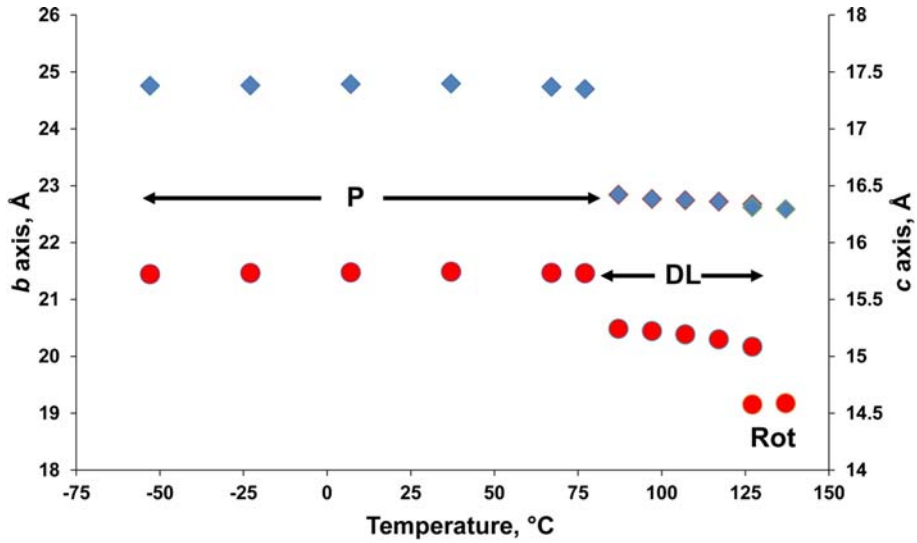

FIG. 10. Variation of *b* (diamonds) and *c* (circles) unit-cell parameters with temperature for penberthycroftite (P), displaced layer phase (DL) and rotated column phase (Rot), resulting from Rietveld refinement of XRD scans obtained by heating penberthycroftite.

diffraction peaks due to the DL phase have not, however, been identified in specimens collected at the Penberthy Croft mine, despite intensive searching. The DL phase is unlikely to persist as a stable mineral, even if local high-temperature conditions existed for its formation by dehydration of penberthycroftite because the transformation is reversible. This was confirmed by running *ex situ* heating experiments on penberthycroftite. The XRD pattern of a sample of penberthycroftite heated to 100°C showed that it had converted predominantly to the DL phase. On cooling to ambient and rerunning the XRD pattern, it was found that the penberthycroftite structure had been restored but the peaks had only about half the height of the peaks before heating, indicating a loss of

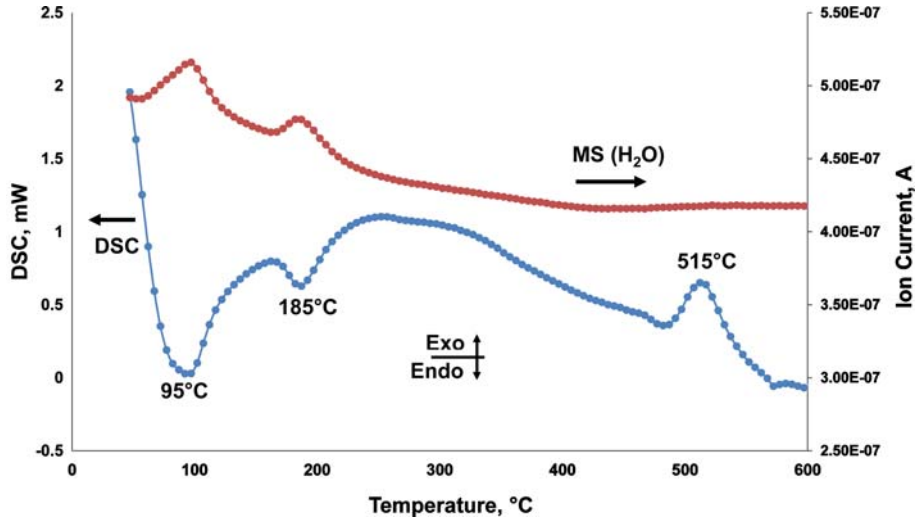

FIG. 11. DSC and MS (for H_2O) curves for penberthycroftite.

https://doi.org/10.1180/minmag.2016.080.126 Published online by Cambridge University Press

long-range ordering. We have previously reported the same behaviour for the related mineral liskeardite, which lost 50% of its crystallinity on heating to 100°C to invoke strong rotation of the framework, followed by cooling to ambient (Grey *et al.*, 2015*b*). The rotation of the [100] columns in forming the DL phase must be accompanied by considerable strain and so it is unlikely that the DL phase will be found in the natural state as a mineral.

Acknowledgements

Part of this research was undertaken at the powder diffraction beamline at the Australian Synchrotron, Victoria, Australia. We thank Yesim Gozukara of CSIRO manufacturing for the DSC/MS measurements.

References

Betterton, J. (2000) Famous mineral localities: Penberthy Croft mine, St. Hilary, Cornwall, England. *UK Journal of Mines and Minerals*, **20**, 7–37.

Buerger, M.J., Dollase, W.A. and Garacochea-Wittke, I. (1967) The structure and composition of the mineral pharmacosiderite. *Zeitschrift fur Kristallographie*, **125**, 92–108.

Evans, J.S.O. (1999) Negative thermal expansion materials. *Journal of the Chemical Society, Dalton Transactions*, 3317–3326.

Grey, I.E., Mumme, W.G., MacRae, C.M., Caradoc-Davies, T., Price, J.R., Rumsey, M.S. and Mills, S.J. (2013) Chiral edge-shared octahedral chains in liskeardite, $[(Al,Fe)_{32}(AsO_4)_{18}(OH)_{42}(H_2O)_{22}]\cdot 52H_2O$, an open framework mineral with a pharmacoalumite-related structure. *Mineralogical Magazine*, **77**, 3125–3135.

Grey, I.E., Kampf, A.R., Price, J.R. and MacRae, C.M. (2015*a*) Bettertonite, $[Al_6(AsO_4)_3(OH)_9(H_2O)_5]\cdot 11H_2O$, a new mineral from the Penberthy Croft mine, St. Hilary, Cornwall, UK, with a structure based on polyoxometalate clusters. *Mineralogical Magazine*, **79**, 1849–1858.

Grey, I.E., Brand, H.E.A., Rumsey, M.S. and Gozukara, Y. (2015*b*) Ultra-flexible framework breathing in response to dehydration in liskeardite, $[(Al,Fe)_{16}(AsO_4)_9(OH)_{21}(H_2O)_{11}]\cdot 26H_2O$, a natural open-framework compound. *Journal of Solid State Chemistry*, **228**, 146–152.

Grey, I.E., Betterton, J., Kampf, A.R., Macrae, C.M., Shanks, F.L. and Price, J.R. (2016) Penberthycroftite, $[Al_6(AsSO_4)_3(OH)_9(H_2O)_5]\cdot 8H_2O$, a second new hydrated aluminium arsenate mineral from the Penberthy Croft mine, St. Hilary, Cornwall, UK. *Mineralogical Magazine*, **80**, 1149–1160.

Harries, J.R. and Ritchie, A.I.M. (1981) The use of temperature profiles to estimate the pyritic oxidation rate in a waste rock dump from an opencut mine. *Water, Air and Soil Pollution*, **15**, 405–423.

Lightfoot, P., Woodcock, D.A., Maple, M.J., Villaescusa, L.A. and Wright, P.A. (2001) The widespread occurrence of negative thermal expansion in zeolites. *Journal of Materials Chemistry*, **11**, 212–216.

Rodriguez-Carvajal, J. (1990) FULLPROF: a program for Rietveld refinement and pattern matching analysis, in: *Proceedings of the Satellite Meeting on Powder Diffraction of the XV Congress of the IUCr*, Toulouse, France, 1990.

Schmitt, B., Bronnimann, C., Eikenberry, E.F., Gozzo, F., Hormann, C., Horisberger, R. and Patterson, B. (2003) Mythen detector system. *Nuclear Instruments and Methods in Physics Research*, **A501**, 267–272.

Wallwork, K.S., Kennedy, B.J. and Wang, D. (2007) The high resolution powder diffraction beamline for the Australian Synchrotron. *AIP Conference Proceedings*, **879**, 879–882.

https://doi.org/10.1180/minmag.2016.080.126 Published online by Cambridge University Press